Water Research X 25 (2024) 100272

Contents lists available at ScienceDirect

Water Research X

journal homepage: www.sciencedirect.com/journal/water-research-x

Overlooked role of long capping time and environmental factors in the plateau lake for impairing lanthanum-modified-bentonite's immobilization to phosphate

Jinhui Wang [a,b], Lina Chi [a], Shuai Liu [a,b], Jiao Yin [d], Youlin Zhang [d], Jian Shen [a,b,c,*], Xinze Wang [a,b,c,*]

[a] School of Environmental Science and Engineering, Shanghai Jiao Tong University, Shanghai, China
[b] National Observation and Research Station of Erhai Lake Ecosystem in Yunnan, Dali, China
[c] Yunnan Dali Research Institute of Shanghai Jiao Tong University, Dali, China
[d] Yuxi Lake Ecological Environment Protection Research and Engineering Management Center, China

ARTICLE INFO

Keywords:
Sediment
Long-term immobilization
Disturbance
Size effect
Competitive coordination

ABSTRACT

Lanthanum-modified-bentonite(LMB) has been applied for eutrophication management as a phosphate(P)-binding agent in many lakes. However, re-eutrophication took place several years or decades later after the first practice of capping due to dynamic environmental factors in the plateau lake. Here, we investigated the effect of long-term capping and integrated environmental factors in the plateau lake including alkalinity, organic matter, disturbance and photodegradation to the LMB immobilization. Long-term LMB immobilization exhibited C accumulation(82.3%), La depletion(53.5%) and lager size effect in the sediment particle, indicating the breakage of La-O-P bonds and the formation of La-O-C bonds over immobilization time. Additionally, pH(8–10) in the plateau lake could enhance the P desorption and decrease P adsorption through electrostatic repulsion enhancement with the zeta potential reduction(7.2 mV). Further disturbance experiment indicated a significant releasing trend of active P and DGT-labile P from the solid phase, pore water to the overlying water after disturbances due to resuspended releasing, particle size and amorphous Fe, Mn and Al's redistribution. Moreover, ^{31}P NMR and EPR results indicated photodegradation after disturbance converted diester phosphate into orthophosphate with long-term LMB immobilization via the oxidation of ·OH in the sediment of the plateau lake. Therefore, management issues for Xingyun Lake may apply to other plateau lakes with low external P input, intermediate depth and intense disturbance.

1. Introduction

Lake eutrophication has become a long-lasting issue that plagues freshwater ecosystems and drinking water safety around the world (Zawiska et al., 2023; Graeber et al., 2024). Internal phosphorus(P) releasing from sediments to the overlying water could aggravate the eutrophication due to the excessive P loading in the lake even after the exogenous P inputs have been controlled efficiently (Ding et al., 2023; Moyle et al., 2024). Multiple sediment remediation technologies have been developed to prevent sedimentary P release, such as dredging, *in-situ* immobilization technique, chemical injection, and bio-treatment technology (Yin et al., 2020). Taking into consideration the fast and safe interception and binding of P released from internal sediment inventories, *in-situ* immobilization using P-sorbent as a capping material is considered to have great potential among the numerous endogenous P remediation technologies (Lin et al., 2023; Zhan et al., 2023). The *in-situ* P-immobilization could not only reduce the TP concentration in overlying water at the initial stage, but also promote the transformation of the exchangeable P to the stable fraction in the surface sediment (Copetti et al., 2016). To date, various P-immobilization materials have been developed and several of them have been applied extensively in laboratory and field experiments ascribed to their superior affinity for P, including aluminum, calcium, lanthanum hydroxides and carbonate, clay minerals, modified clay minerals (iron-modified zeolite, zirconium-modified bentonite, iron-modified attapulgite, lanthanum modified bentonite (LMB)), etc. (Yin et al., 2017; Yin et al., 2020; He

* Corresponding authors.
E-mail addresses: sjlnts@sjtu.edu.cn (J. Shen), xinzewang@sjtu.edu.cn (X. Wang).

https://doi.org/10.1016/j.wroa.2024.100272
Received 27 September 2024; Received in revised form 22 October 2024; Accepted 28 October 2024
Available online 29 October 2024

et al., 2022; Guo et al., 2024). However, as widely recognized, the immobilization is not long-lasting and needs repeating. Re-eutrophication took place several years or decades later after the first practice of capping due to dynamic environmental factors.

According to previous studies, the efficacy of *in-situ* immobilization agents might be impaired significantly over time by both intrinsic (such as anoxia conditions and organic substance accumulation) and extrinsic (like high water temperature, disturbance-induced resuspension and reinforced hydrodynamic velocity, etc.) conditions of the lake environment. Münch and his group reported that re-eutrophication of Terra Nova Lake (the Netherlands) two years later after the covering of $FeCl_3$, might be ascribed to the excessive organic matter competition and frequent sediment mixing (Münch et al., 2024). Similarly, re-eutrophication of Barleber Lake (Germany) even 30 years later after the covering of $Al_2(SO_4)_3$ might be attributed to the combined factors of loss of aluminum-P adsorption capacity, anoxia condition and high water temperatures (Dadi et al., 2023). Another investigation in the six Danish lakes treated with poly-Al chloride in 9 years disclosed that the translocation of Al by resuspension and furious bottom-currents might explain the intensified re-flocculation of Al-P from the sediments (Egemose et al., 2013). Recently, due to superior adsorption capacity, low cost, facile preparation and environmental friendliness, there has arisen a growing interest in adopting commercialized LMB as the capping materials for lake eutrophication remediation in 200 waters (e.g. Otterstedter See, Silbersee, Rauwbraken, H. G. Eiland, Mere Mere and Hatchmere) (Dithmer et al., 2016) and achieved various success due to ion exchange in the interlayer structure of the bentonite and surface adsorption of La^{3+} to $H_nPO_4^{n-3}$(n=0, 1, 2 and 3). However, given the shorter application time, better stability and insolubility in nature of LMB compared to iron and aluminum salts, whether re-eutrophication would happen to these real practices is still doubtful.

In other words, the effects of intrinsic and extrinsic environmental factors on P releasing from the surface sediment treated by LMB in real scenarios need further concern. Moreover, previous investigations on the long-term effects of *in-situ* internal-P-immobilization focus on the lakes located in plain rather than plateau areas. Owning to the lower atmospheric pressure and more furious wind disturbance caused by high altitude in contrast to the plain lakes, the physical active barrier of the sediment in plateau lakes is more likely to be destroyed (Wang et al., 2017) with the change of redox potential at the sediment water interface (SWI) (Wu and Hua 2014; Jalil et al., 2017), not to mention the photochemical reaction of organic phosphate (OP) triggered by the higher level of solar irradiation (Guo et al., 2020). This paper focused on Xingyun Lake, a hypertrophic shallow lake (with an average depth of 6 m) at the Yunnan-Guizhou Plateau within the southwestern border area of China. LMB was added in the strength of 144 g/m^2 in May 2019, November 2019 and June 2020 (http://www.phoslock.cn/post/208468/) which resulted in the increase of total La concentrations in the solid phase among the top 10 cm sediment (Fig. S1a) and consequential decrease of TP concentration of overlying water from 0.322 mg/L (inferiority Class V) to 0.077 mg/L (Class III) in a short period (Fig. S2). It was not the end of the story. An explosive growth of algal blooms happened again with the deterioration of water quality in 2023 and 2024, which prompted immediate investigations into the potential causes of the re-eutrophication (TP, SRP concentration and release flux in Fig. S2,S3). It is well recognized that Xingyun Lake was featured as high alkalinity and COD (especially humic acid and algae-derived organic matter, AOM) due to long water exchange cycles (Zhou 2016; Zeng et al., 2022b). It has been reported that HCO_3^-, humic acid and AOM could weaken the removal performance of adsorbent in the natural water (Wang et al., 2022a; Wang et al., 2023; Wen et al., 2023). High alkalinity leads to relatively high pH(8–10) and HCO_3^- concentration (200–400 mg/L), which possibly tends to weaken the removal performance of P. Studies so far remain two questions that have as yet no clear answer: Could environmental factors of plateau lake (like Xingyun Lake) affect LMB immobilization and what are the potential changes in the sediment after the long-term immobilization? The ability of researchers and governments to anticipate, mitigate, and restore eutrophic freshwaters in a cohesive, integrated manner suffers from key uncertainties in our understanding.

Hereby, the goal of this study was to evaluate how the immobilization time and plateau lake factors affect the P-immobilization of sediment with LMB. Specifically, we methodically explored and elucidated the underlying mechanisms: i)phase dynamics of the surface sediment with the long-term LMB capping by SEM, XRD and XPS; ii)effects of alkalinity ions (OH^-, HCO_3^-), humic acid and algae-derived organic matter (AOM) on immobilization by zeta potential; iii)effects of different disturbances on the immobilization in the sediment vertical profile with long-term LMB capping associated with the particle size distribution and amorphous Fe, Al, Mn in the vertical profile of the sediment; iv)irradiations on the immobilization effect in the sediment with long-term LMB capping after disturbance by ^{31}P NMR and EPR. Therefore, our work provides theoretical support for reevaluating the feasibility of LMB application to control internal P pollution in high-altitude lakes with long immobilization time, intermediate depth and strong disturbance.

2. Results and discussion

2.1. Immobilization time effect and mechanism

To examine the surface morphology and element distribution changes of sediment over immobilization time, SEM and EMI characterizations of LMB treated sediment after short-term immobilization (LSS) and LMB treated sediment after long-term immobilization (LSL) were employed. Fig. 1(a,b) showed the lamellar banded morphology in both LSL and LSS samples. However, LSS exhibited a plain fine structure with more pores and a rougher surface with higher crystallinity, whereas LSL revealed more significant agglomerations and smoother surfaces, In addition, elemental images also indicated C(Fig. 1g,1h) more evenly distributed after the long-term immobilization. Above phenomenon probably derived from long-term organic matter and carbonate accumulation from the lake. La(Fig. 1c,1d) and P(Fig. 1e,1f) content significantly reduced and confirmed the scarcity of La (the bonding sites of P) and explained one of the reasons why immobilization capability was impaired and SRP/TP of LSL tended to release to the overlying water compared with that of LSS (Fig. S4).

To further elucidate the evolution of phase composition and chemical bonding, XRD and XPS analyses of LSS and LSL were conducted. As shown in Fig. 1i, the LSS and LSL samples exhibited the dominant content of SiO_2 and distinct crystal structures of $LaCl_3$ and $Mg_{.064}Ca_{.936}CO_3$ (Copetti et al., 2016), respectively. It was worth noting that $LaCl_3$ peak of LSL vanished while peaks of calcium carbonate and calcium magnesium carbonate gradually emerged along the extension of the immobilization time, which might be attributed to the soil formation related carbonate under karstic landforms (Jin et al., 2021; Peng et al., 2021). These findings were consistent with the XPS full-spectrum semi-quantitative analysis, which showed an 82.3% increase in the C atomic ratio, 53.5% decrease in the La atomic ratio in LSL samples compared to LSS samples (Table S1). The La 3d orbital fine spectrum analysis revealed a decrease in the integration area and the changes of chemical bonds of La after long-term immobilization (Fig. 1k). The four peak positions of the La 3d orbital after long-term immobilization changed in different degrees compared to that in LSS, with the corresponding peak binding energy (BE) shifted from 855.65, 852.31, 838.88 and 839.23 eV in LSS to 856.36, 852.84, 839.23 and 835.82 eV in LSL. The C 1 s orbital fine spectrum (Fig. 1o) also indicated that the C integration area of LSL was significantly larger than that of LSS, with the proportion of carbonate increasing from 8.2% to 12.9%, and the proportion of C—O bonding rising from 17.2% to 44.4%. The P 2p orbital fine spectrum (Fig. 1n) demonstrated that the relative area at P $2p_{3/2}$ decreased from 43.8% in LSL to 36.6% in LSS, probably derived from the decomposition of OP and the release of inorganic phosphorus after

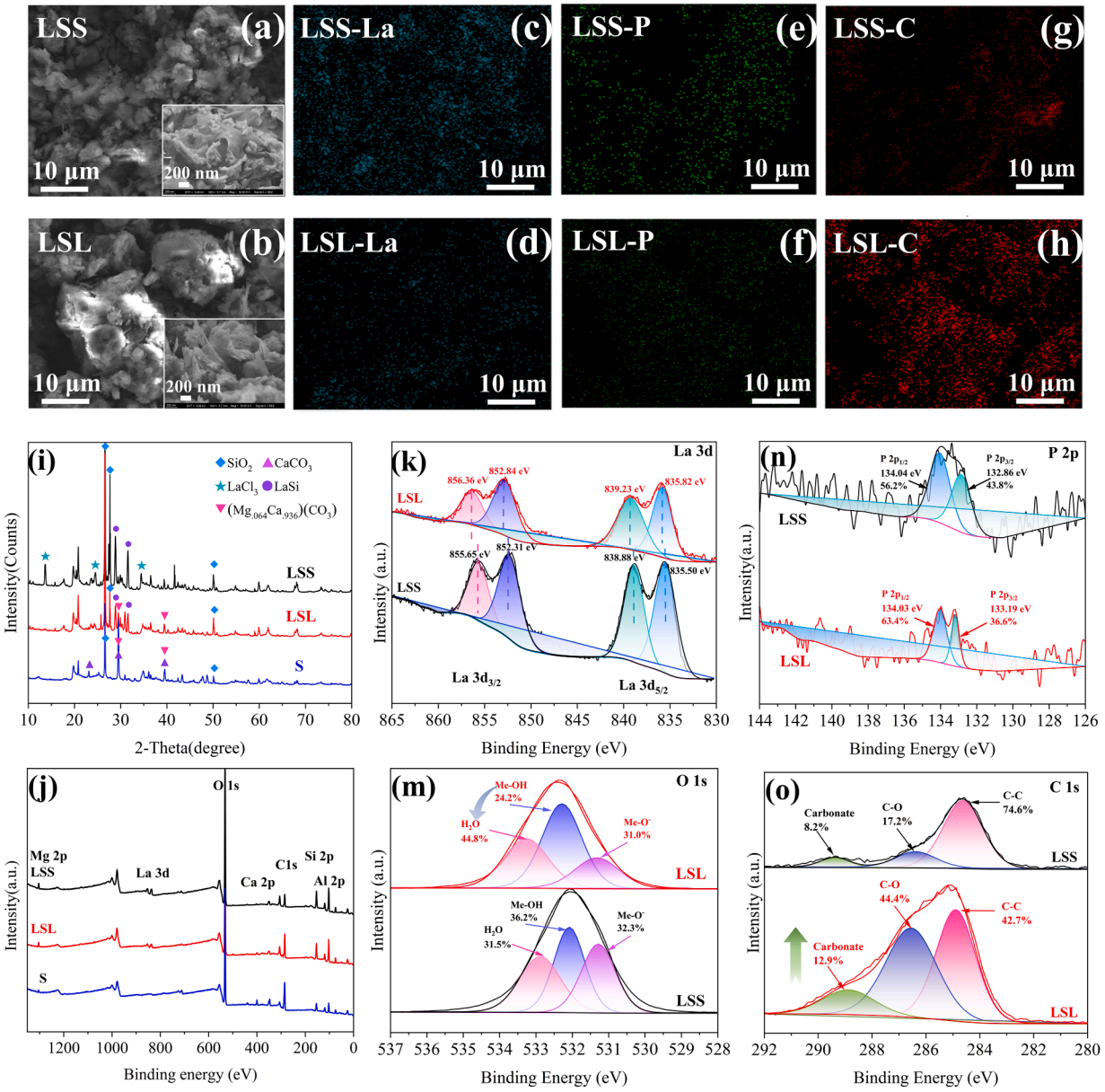

Fig. 1. Scanning electron microscopy (SEM) images of LSS (a) and LSL(b) and elemental mapping images (EMI) of La(c, d), P(e, f) and C(g, h); XRD of S, LSS and LSL; XPS of survey spectra(a), La 3d(k), O 1s(m), P 2p(n), and C 1s(o); LMB treated sediment after short-term immobilization(LSS), LMB treated sediment after long-term immobilization(LSL), untreated sediment(S).

long-term immobilization. With a comparison of the 132.9 eV peak assigned to $NaH_2PO_4{\cdot}2H_2O$ (Mallet et al., 2013) in LSS and LSL samples, we speculated that the adsorbed $H_nPO_4^{n-3}$ in LMB was released to the overlying water during the long-term immobilization process, which was in a good agreement with the evidence of breakage of the La-O-P bond from O1s orbitals spectrum. According to Fig. 1m, metal hydroxyl in the adsorbed oxygen was reduced from 36.2% in LSS to 24.2% in LSL and replaced with La-O-C bonds due to the stronger carbonate's binding capacity for La($Ksp(La_2(CO_3)_3=3.98\times10^{-34}\ll Ksp(LaPO_4)=10^{-24.7}\sim10^{-25.7}$) and the ligand exchange in La complexion between CO_3^{2-}/HCO_3^- and $H_nPO_4^{n-3}$ during the aging process (Zhan et al., 2023). Overall, our study confirmed that the breakage of La-O-P bonds and the formation of La-O-C bonds in the long-term LMB immobilization, which was in line with the evidence of P decrease and C increase demonstrated in EMI.

In addition, it was found that the particle size distribution of the LMB treated sediment changed over the immobilization time, which possibly influenced the capping performance and explained the related effect mechanism. According to the particle size analysis of LSS and LSL in the depth of 0–2 cm below the SWI, the particle size(D_{50}) of LSL was about 2.561 μm more than 20 times larger than that of LSS, while S/V (specific surface area) of LSL was 22.9% smaller than LSS after long-term LMB immobilization. Furthermore, the percentage of particle size above 63 μm increased by 3.9%, with that below 8 μm decreased by 4.2% (Table S3), indicating the downsize of contact area between LSL and the water above the capping layer and in pore water. The size effect of sediment particle explained another reason why SRP(0.06 mg/L) and TP (0.09 mg/L) of LSL were higher than SRP(0.03 mg/L) and TP(0.05 mg/L) of LSS in the overlying water (Fig. S4). It was also responsible for a higher passivation effect in LSS compared with LSL under the same minor disturbance due to smaller particle size and larger contact area (S/V).

2.2. Alkalinity and organic matter effect

To explore the pH-dependent effect of raw sediment(S), LSS and LSL's immobilization performance to P, adsorption, desorption amount and zeta potential under different pH were determined (Abdellaoui et al., 2021). As shown in Fig. 2(a, b), there exhibited a similar tendency for all three samples of S, LSS and LSL with their P adsorption amount decreased and the desorption amount increased with pH rising from 4 to 12, especially obvious at the pH range of 9–12. With the pH ranging from 8 to 10 (the regular pH range of Xingyun Lake), the P adsorption amount of LSL, S and LSS decreased by 9.5%, 7.1% and 3.3%, respectively, while the P desorption amount raised by 107.9%, 42.2% and 50.0%. On the other hand, in the pH range of 4–12, S, LSS and LSL were all negatively charged with their ζ potentials declining with the increase of pH value (Fig. 2c), ascribing to the pH-independent negative charges associated with isomorphous substitution of Si^{4+} with the cation of lower valence like Al^{3+} and Fe^{3+} and pH-dependent negative charges from deprotonation of Si-O-H on the clay surface. With the pH adjustment from 8 to 10, the zeta potential of S, LSS and LSL decreased 4.0, 7.2 and 6.8 mV respectively. Such a decline in the alkaline microenvironment would cause more surface negative charges, stronger electrostatic repulsion and weaker ions exchange toward $H_nPO_4^{n-3}$ of LMB treated and untreated sediment. The values of ζ potential of S <LSL <LSS colloidal system also indicated less stability in the untreated sediment and LSL than LSS. Therefore, it was the elevated pH that increased the negative charge of the colloid surface strengthened the electrostatic repulsion and ions exchange between $H_nPO_4^{n-3}$ and LSL, leading to the impaired P-adsorption on LSL compared to LSS under high pH.

As we know, the presence of carbonates and organic ligands (including HA and AOM) in natural waters may hinder the removal performance of adsorbent to P. We further explored the influence of concentrations fluctuation of HCO_3^-, AOM and humic acid on P adsorption on LMB under pH range of 8–10 to simulate the alkaline environment in Xingyun Lake. The results showed that high concentrations of HCO_3^- and AOM(Fig. 2d,2f) had a significant inhibition effect on raw LMB's adsorption of P in comparison to humic acid (Fig. 3e). As the concentrations of HCO_3^- increased from 0 to 1000 mg/L and AOM rose from 0 to 36 mg/L, the adsorption rate of LMB dropped from 99.8% to 38.6% and 39.8%, respectively. In comparison, the adsorption rate of P fluctuated up and down slightly between 95.7% and 79.0% with the concentration of HA ranging from 0 to 36 mg/L. The inhibition effect of HCO_3^- was related to $K_{sp}[La_2(CO_3)_3]<<K_{sp}[LaPO_4]$ at the temperature of 25°C (Reitzel et al., 2017). Plus, as mentioned above, the upward adjustment of pH value attributed to the increase of HCO_3^- concentration gave rise to the stronger electrostatic repulsion to anion, which synergistically fortified the inhibition to P adsorption. Regards to AOM and HA, it was probably due to the less homogeneity of the organic carbon in AOM-associated co-precipitates that happened a labile complexion of AOM with P but an inhibition to P adsorption (Wen et al., 2023). Specifically, the organic carbon in the AOM-Fe-P co-precipitates was not homogeneous with more carboxyl groups and greater electrostatic repulsion than that in HA-Fe-P, which led to an unstable bonding of AOM with P and therefore an inhibition of P adsorption to some degree. Based on observed values of overlying water in Xingyun Lake in April 2023, the concentrations of HCO_3^-, AOM and humic acid were 218.7, 9.1 and 4.3 mg/L, respectively. Therefore, there were two predominant factors in alkalinity and AOM that could contribute to the P inhibition effect of LMB: electrostatic repulsion and competitive adsorption, which was also applicable for other plateau rift lakes with high alkalinity and organic matter accumulation.

2.3. Disturbance dynamics

Disturbances play a key role in the P diffusion from SWI because solid-phase active P could be replenished into the pore water and be released into the overlying water due to due to solid-liquid mass transfer and resuspension caused by disturbances (Yang et al., 2023). Furthermore, resuspension caused by disturbances could remold vertical redistribution of amorphous Fe, Mn and Al due to the subsequent redistribution of particle size in the sediment vertical profile (Wang et al., 2022b). As a typical high-altitude lake in China, the main factors leading to disturbances in Xingyun Lake are subjected to frequent wind (with an average linear velocity of 0.95 m/s) and hydraulic processes (with an average linear velocity of 0.40 m/s) according to the empirical equations in Text S3 (Liu et al., 2021). Therefore, the following discussion would be focused on P diffusion on the SWI of LSS and LSL in the water phase, sediment solid phase and pore water phase under the major (MA) and minor(MI) disturbances.

LSL no matter under major disturbance (LSL-MA) and minor disturbance (LSL-MI) showed releasing trends of SRP and TP into the overlying water (Fig. 3a, 3c) with SRP and TP of LSL-MI increased 0.020 and 0.026 mg/L, and those of LSL-MA increased 0.033 and 0.031 mg/L

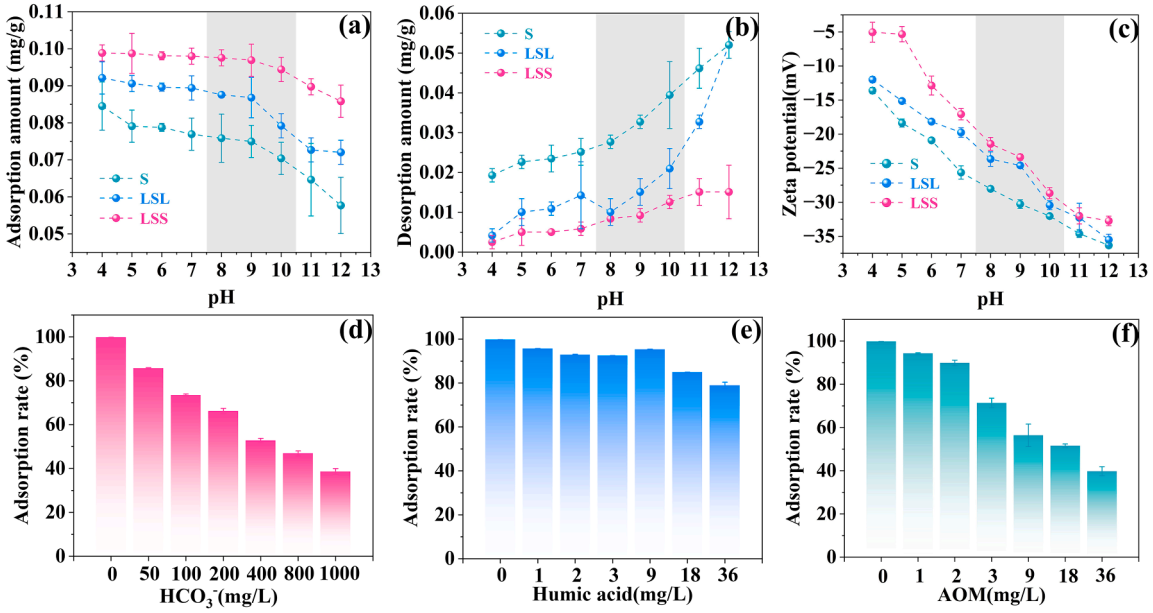

Fig. 2. Adsorption amount(a), desorption amount(b) and zeta potential(c) of S, LSS and LSL to P, HCO_3^-(d), HA(e) and AOM(f) effect on LMB adsorption rate of P.

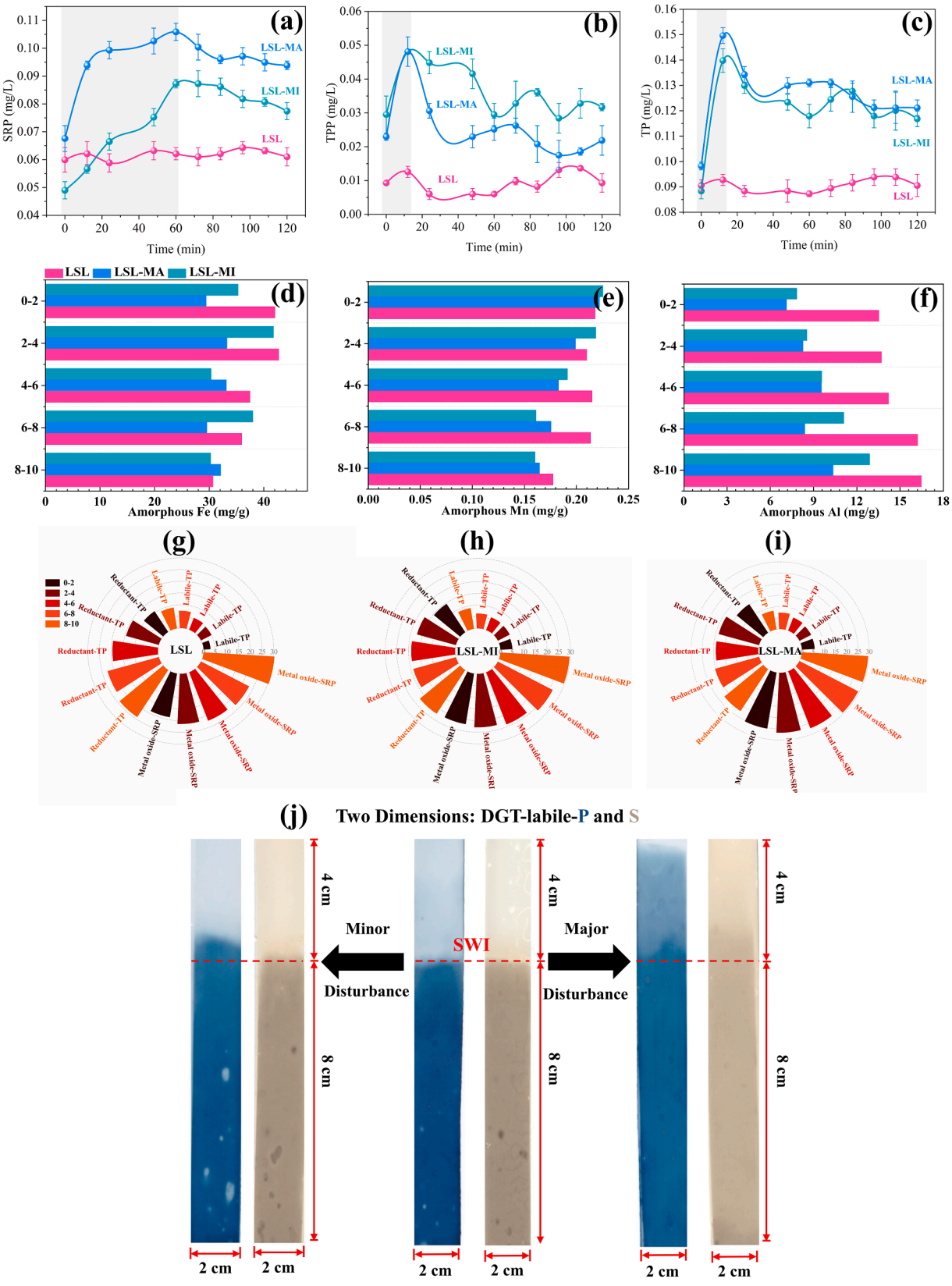

Fig. 3. SRP(a), TPP(b) and TP(c) in overlying water after minor/major disturbance; Amorphous Fe(d), Mn(e), Al(f) and DGT-labile P and S(j) in the vertical profiles of LSL after minor/major disturbance; Active P fractions in the vertical profiles of sediments with long-term LMB immobilization after the no(g)/minor(h)/major(i) disturbance: LMB treated sediment after long-term immobilization with the minor disturbance(LSL-MI), LMB treated sediment after long-term immobilization with the major disturbance(LSL-MA).

compared with non-disturbed groups, respectively. In terms of kinetics, SRP and TP in all the disturbance groups of LSL were released quickly during the initial stage followed by a relatively slow process with SRP stabilized at 0.08 mg/L (increased by 33.3% compared to the initial concentration) in LSL-MI and over 0.09 mg/L(56.7%) in the LSL-MA, TP stabilized at 0.11 mg/L (22.2%)in LSL-MI and 0.12mg/L(34.3%) in the LSL-MA. Interestingly, LSL-MA had identical TP while higher SRP and lower TPP compared with LSL-MI (Fig. 3b), implying major disturbance could accelerate the transfer rate of TPP to SRP by improving interaction frequency between the sediment and overlying water. The SRP of LSL-MA reached the equilibrium after 72 min, while LSL-MI reached the equilibrium within 60 min. Therefore, compared with minor disturbances, major disturbances could cause higher contact frequency and longer resuspension time of the sediment particles in the overlying water, which provided a longer window period for P in the solid state to release into water-phase before the settlement.

The presence of DGT-labile-P in the sediments with long-term LMB immobilization (Fig. 3j) implied that P still can be leached from the sediment or pore water to compensate for the relatively lower concentration of dissolved P in the overlying water (Ding et al., 2010). According to the color variations which represent the differences of accumulated DGT-labile-P, a significant diffusion gradient of the DGT-labile-P could be found in the control group and the MI group, but not in the MA group. The DGT-labile-P cumulative flux of LSL-MA was higher in the overlying water and much lower than those of LSL-MI in the pore water, suggesting the resuspension caused by major disturbance promoted DGT-labile-P homogenous redistribution and aggravated risk of phosphorus release from the pore water in the two-dimensional sediment plane. Although there demonstrated release of the DGT-labile-P in the depth of 0–4 cm below the SWI under both levels of disturbance, it was more evident in LSL-MA, which was consistent with the SRP and TP releasing trend into the overlying water in LSL-MA. The concentration of DGT-labile-P in LSL-MA was higher than that of LSL-MI in the depths range of 0–4 cm, which implied that the DGT-labile-P releasing rate from LSL-MA was higher than that of LSL-MI and both exceeded the passivation rate of LSL. It was found that the major disturbance gave rise to increased P-releasing flux with P releasing spectrum even extended to 8 cm below the SWI. As far as S^{2-} was concerned, the concentration of LSL-MA decreased significantly along the depth under SWI due to its more sensitive nature to dissolved oxygen and Eh (Lin et al., 2023). Lower S^{2-} concentration in LSL-MA further implied that major disturbance promoted the increase of ORP throughout the whole vertical sediment profile (Table S2). However, higher ORP ought to decrease the DGT-labile-P release (Li et al., 2019), which was opposite of the observed DGT-labile-P distribution. It demonstrated that the P releasing effect of disturbance surpassed the immobilization impact of increased ORP in this study. Thus, the variation of ORP was not the main reason for the DGT-labile-P change in the vertical profile of sediment after disturbance in this study.

To further explore the reason of DGT-labile-P release in the vertical profile of sediment, active P in the sediment phase (mainly includes labile-P, reductant-P and metal oxide-SRP) was determined according to Hupfer's fractionations (Hupfer et al., 1995). Above P contents increased with the rise of depth in all groups (Fig. 3g,3h,3i), manifesting a certain concentration diffusion gradient ($p < 0.05$) while the principle of inert P was the opposite (Fig. S5). The content of active P was dramatically changed by the disturbance in the vertical profiles, especially in the depths 0–4 cm below the SWI. The active P content in the sediments with long-term LMB immobilization presented the following rules: LSL-MI was lower than that of LSL-MA but higher than that of LSL. Specifically, the labile-P, reductant-P and metal oxide-SRP of LSL-MI increased by 17.5%, 10.7% and 11.2% compared to LSL, respectively. The labile-P, reductant-P and metal oxide-SRP of LSL-MA increased by 24.8%, 17.8% and 29.1% compared to LSL, respectively. Meanwhile, C.V of all P fraction content lessened after minor and major disturbance and that of major disturbance was lowest. Especially for C.V. of the metal oxide-P, it decreased from 0.164(LSL) to 0.112(LSL-MI) and 0.059 (LSL-MA) in the depth of 0–4 cm below the SWI, indicating the disturbance and resuspension promoted P fraction distribution homogenization. Relatively high active P homogenization in LSL-MI and LSL-MA suggested the low passivation rate of active P and the high diffusion rate of active P from the bottom to the upper sediment. Active P would be released to compensate for the deletion of pore water after the disturbance when the content of dissolved P in pore water diminished (Pan et al., 2019).

The vertical distributions of amorphous Fe(Fig. 3d), Mn(Fig. 3e) and Al(Fig. 3f) in sediments could reflect the solidification capability of sediments to pollutants (Li et al., 2023). The results demonstrated that the above distributions had the following characteristics. The content of amorphous Fe, Mn and Al and their C.V at different depths of the sediment gradually decreased with the reinforcement of the disturbance. In detail, the average amorphous Fe content of LSL-MI and LSL-MA shrank by 7.0% and 16.6%, the average amorphous Al content of LSL-MI and LSL-MA shrank by 32.6% and 41.1%, the average amorphous Mn content of LSL-MI and LSL-MA shrank by 9.0% and 10.0% in the whole vertical profile. It was related to the redox potential change and the increase of the interaction frequency between the bottom and the top of sediment phases (Table S2) (Wang et al., 2022b).

To explore the reasons of amorphous Fe, Mn and Al distribution under disturbance, the particle size distribution in the whole vertical sediment profile was determined in Table S3. The value of D_{50} in LSL-MI (2.56 μm) was lower than that of LSL-MA(3.84 μm) after resuspension while higher than that of LSL-MA(2.72 μm) in the depths of 0–2 cm below the SWI. The value of S/V in LSL-MI(0.356 m^2/cm^3) and LSL-MA (0.258 m^2/cm^3) increased compared with LSL(0.405 m^2/cm^3) in the depths of 0–2 cm below the SWI, indicating less contact area between surface sediment and overlying water body after the disturbance. In addition, the proportion of particle size below 8 μm and S/V decreased while the proportion of D_{50} and >63 μm increased in the shallow sediment (0–6 cm below the SWI) with the rise of disturbance, which was conforming to the principles of resuspension. According to the statistical correlation analysis (Fig. S4), S/V exhibited a negative correlation with depth and particles >63 μm, but a positive correlation with amorphous Mn. Our results confirmed that there is a positive correlation between <8 μm clay and Fe distribution while a negative correlation between >63 μm clay and Fe and Mn distribution (Wang et al., 2022b). Considering the vertical pH results, disturbance can lead to the resuspension of sediment solid granules and sediment homogenization from bottle to top, which can cause variations in particle size and a shift in pH towards alkalinity, which can affect the levels of amorphous Fe, Al and Mn in the sediment.

Therefore, disturbance affected the distribution of amorphous Fe, Mn and Al in sediment solid phase particles over vertical profiles for two main reasons: redistribution of particle size and broadening of the alkaline microenvironment. As it was well known that the screening effect resulting from the frequent wind or hydraulic disturbances might lead to size redistribution, the larger particles tend to be buried at the surface sediment along the duration of immobilization (lower C.V in Table S3), which resulted in low amorphous Fe, Mn and Al loading and DGT-labile-P increase (Shen et al., 2023). As a result, the relatively more anaerobic environment on the bottom facilitated the release of amorphous Fe and Mn in those larger particles, which was confirmed by the variation of vertical profile of amorphous Fe, Mn, Al in LSL under major and minor disturbance compared with those in LSS (Fig.3 and Fig. S4) (Wang et al., 2022b). Furthermore, the vertical pH gradient caused by disturbance was narrowed, disrupting the acidic microenvironment at the sediment's bottom (Table S2) and leading to an increase in alkalinity and the reinforcement of electrostatic repulsion between the sediment and phosphate (He et al., 2022). The decrease in these key substances in the surface sediment can weaken the binding of active P in the sediment solid phase and promoted the DGT-labile-P release, allowing it to diffuse into the pore water and even into the overlying water body.

2.4. Photochemical effect with disturbance

The SRP and DOP curves of the dark group were approximately parallel, and the concentration was relatively stable at 0.0400 mg/L (Fig. 4a). Both weak illumination and strong illumination showed a trend of SRP release in LSL within 70 min, SRP and DOP of the whole groups remained during the stage of 70–90 min, indicating the photodegradation rate was higher than LSL passivation rate. The stronger the illumination, the more the releasing rate of SRP and the greater the degradation amount of DOP. The kinetic curves were all S-shaped, which can be roughly divided into three stages (initial, logarithmic and stable stages). SRP of the weak illumination group increased fast during the stage of 30–70 min by 0.0225 mg/L (Fig. 4c) and that of the strong illumination group increased quickly during the stage of 20–70 min by 0.0373 mg/L compared with the initial concentration (Fig. 4b). The DOP of the weak illumination group was reduced by 0.0237 mg/L and that of the strong illumination group was reduced by 0.0372 mg/L compared with the initial.

To characterize the changes of OP components in the aquatic environment, ^{31}P NMR spectrums of the surface sediment before and after the illumination were determined. It can divide the extracted P by NaOH-EDTA into four forms (Kong et al., 2020), including orthophosphate(a), monoester phosphate(b), diester phosphate(c) and pyrophosphate(d) as shown in Fig. 4g. The chemical shifts of orthophosphate and monoester phosphate which were bound with the high electronegativity groups were in the low field, and the chemical shift of diester phosphate and pyrophosphate were bound with the low electronegativity were in the high field. The proportion of orthophosphate before and after illumination was the highest, orthophosphate monoester and pyrophosphate were next, and the lowest was orthophosphate diester. Four groups of characteristic peaks all appeared before and after photolysis, in which the monoester phosphate and diester phosphate decreased by 3.8% and 7.6% after photolysis, and the orthophosphate and pyrophosphate increased by 7.6% and 1.3% after photolysis. The surface agglomeration phenomenon before photolysis was more obvious, and the fine structure after photolysis was gradually opened and the smooth structure was destroyed. This indicated that carboxyl or hydroxyl groups may be generated on the surface after photolysis. As shown in the SEM (Fig. 4i,4j), the surface agglomeration was more pronounced before the irradiation, while the fine structure gradually unfolded and the smooth structure was destroyed after the irradiation. In the mapping image (Fig. 4k-o), the distributions of the C and P elements became sparser after the irradiation, suggesting there may exist the degradation of organic phosphorus.

Prior to photochemical effect, microbiological factors were considered to play a possible role in degrading OP. C.V of APA enzyme decreased with the extension of illumination time, indicating the systems gradually tended to be stable and the microorganisms gradually adapted to the light environment (Fig. 4d-f). Nevertheless, there were also following differences in the two groups. APA enzyme activity gradually declined with the increment of illumination intensity, concurrently elevating C.V of APA and the inherent instability of enzyme activity. It was reported that Fenton-like reaction on the surface of iron-bearing minerals produces a large amount of hydroxyl radicals (Wang et al., 2024), which inhibited the activity of the APA enzyme (Sheng et al., 2023). Therefore, the biological contribution of APA enzyme to DOP decrease in the sediment was excluded in the irradiation experiments.

To further clarify electron transferring and reactive oxygen species during the photochemical process, EPR of resuspend sediment after 0, 10 and 30-min illumination was tested. The typical plot of hydroxyl radicals(·OH) bound with DMPO was a four-line spectrum at the intensity ratio of 1:2:2:1 with the hyperfine splitting constants of 14.89 G (Wang et al., 2024). As shown in Fig. 4h, EPR for 0 min was basically signal noise which had no signal peak corresponding to ·OH. In comparison, it was obviously observed that four DMPO—OH symmetrical peaks appeared in the 10 min and 30 min curves, indicating ·OH attacked the ester bond of monoester phosphate and diester phosphate as reactive oxygen species during the photodegradation. The ratio of the DMPO peak integral area of the 10 min and 30 min EPR curves in the two photolysis processes was approximately 1:2, indicating that the number of ·OH and oxidative degradation performance gradually decreased as time went on. ·OH had a wide range of sources in the aquatic environment, where nitrite, nitrate and DOM contributed 0.2–24.8%, 0.1–8.8% and 70.0% of ·OH formation in the water, respectively (Xu et al., 2020). Fe-smectite in the sediment also occupied ·the considerable portion in the ·OH formation related Fe(II) species (Du et al., 2021). Additionally, ^{3}CDOM* could yield ·OH, H_2O_2, $^{1}O_2$, and O_2^- through a series of reactions in the photodegradation process, whose effects were also cannot be ignored (Sharpless and Blough 2014) due to high COD in Xingyun Lake, which were similar with other trophic lakes (Xu et al., 2020; Du et al., 2021; Guo et al., 2023).

3. Materials and method

3.1. Sampling and preparation

The overlying waters and top 10 cm sediments below SWI (surface sediments) were collected using a water sample and a grab sampler in April 2023 from Xingyun Lake, located in the Yungui Plateau (N3:102°47.07′ E, 24°21.96′ N and S7:102°46.31′ E, 24°20.82′ N, sampling sites and La content shown in the Fig. S1c), southwestern China. As follows, the samples were stored in a polytetrafluoroethylene bucket and then moved to the refrigerator at 4 °C until use. The sediment located at N3 and S7 were viewed as LMB treated sediment after long-term immobilization(LSL) and blank sediment because of the current La content (Fig. S1a), prevailing wind direction and hydrological characteristics (Liu et al., 2021). LMB was purchased from Phoslock Water Solutions Limited, Australia. The sediment of N3 was homogenized, sieved through a 0.6 mm sieve and then backfilled into Perspex tubes. The sampled water was filtered through a cellulose acetate membrane with the pore size of 0.45 μm and the permeate was aerated at the temperature of 25 °C. It was added to the sediment core to balance the amount of water evaporated daily during 25-day pre-incubation. The overlying water of the sediment core was sampled every day for the determination of SRP and TP.

To mimic real conditions in the Xingyun Lake, the sediments of N3 and S7 were backfilled into Perspex tubes to form a series of small sediment cores (h = 28 cm; $Ø$=10 cm), with 18 cm of sediment and 10 cm of water. For LMB treated sediment after short-term immobilization (LSS), 0.68 g of Phoslock® was mixed with 100 mL of lake water and added to each core of S7 as slurries on day 0 based on the actual LMB dosage in Xingyun Lake, followed by 30 days' immobilization. Similarly, they were aerated at constant temperature and added with the appropriate amount of overlying water to balance the amount of water evaporated daily.

3.2. Microcosm experiment

3.2.1. Disturbance experiment

The Perspex tubes were connected to an electric stirrer after a 25-day pre-incubation to form the disturbed groups, whose paddles were placed 1.5 cm above the SWI (Funes et al., 2021). On the 26th day, the sediment cores with minor disturbance(MI) were exposed to the rotational speed of 133±5 rpm (linear velocity: 0.4 m/s) for 15 min. According to the empirical equations and published methods (Text S1) (Jalil et al., 2017; Funes et al., 2021), the major disturbance groups(MA) were exposed to the rotational speed of 315±5 rpm (linear velocity: 0.95 m/s) for 15 min. Then the pH, ORP and temperature of the overlying water were immediately determined by the electrode methods. TP, SRP and DTP of the overlying samples were sampled and determined at the corresponding time points using ammonium molybdate spectrophotometry.

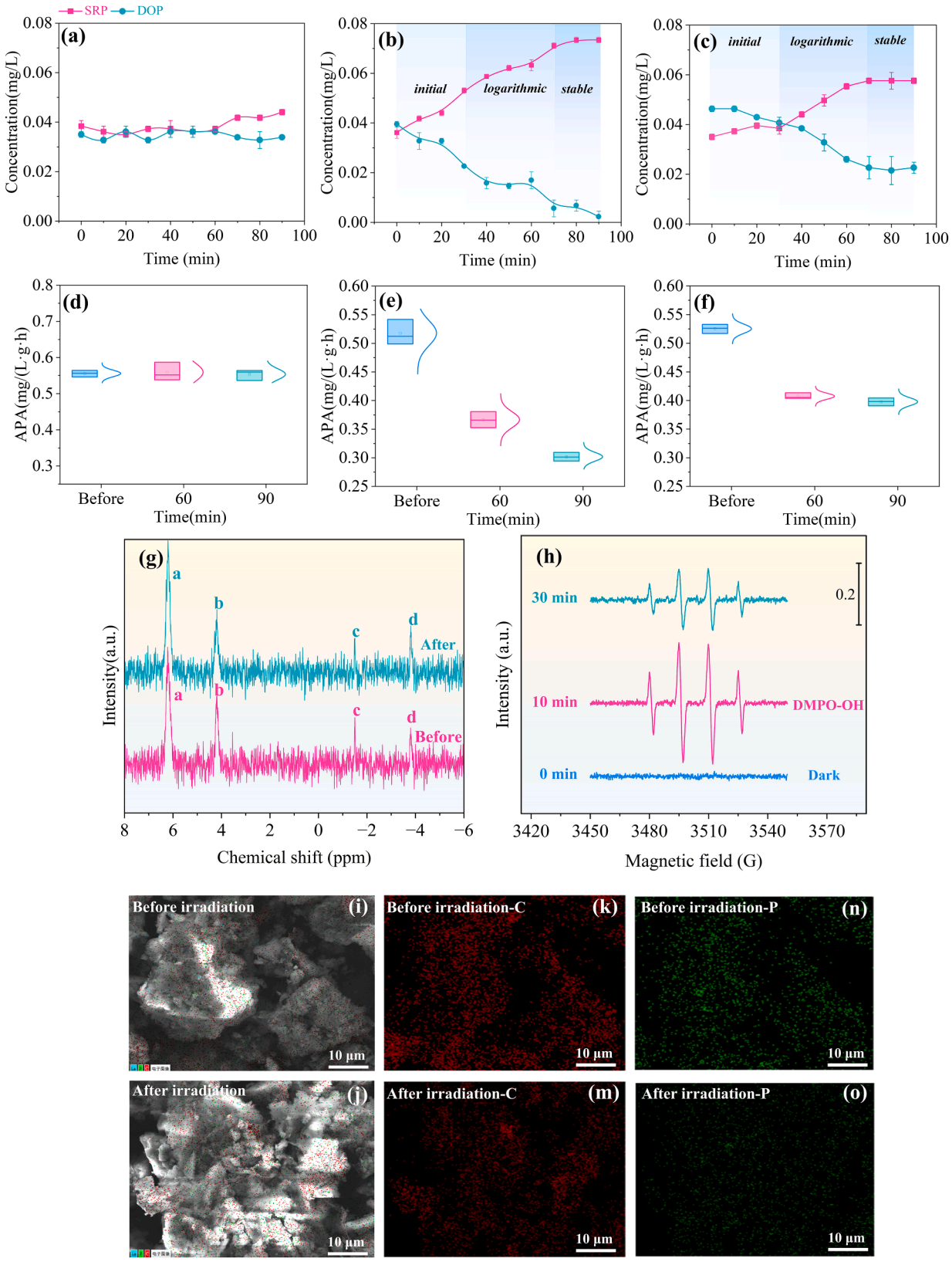

Fig. 4. SRP and DOP in the microcosm groups at the dark(a), strong(b) and weak(c) illumination; APA in the microcosm groups with long-term LMB immobilization at the dark(d), strong(e) and weak(f) illumination; ^{31}P-NMR spectra of NaOH-EDTA extracts of the resuspended sediments (0–2 cm) before and after illumination(g) orthophosphate(a), monoester phosphate(b), diester phosphate(c) and pyrophosphate(d); EPR spectra for the detection of ·OH in the presence of 0.14 M DMPO(h); Scanning electron microscopy(SEM) images and elemental mapping images (EMI) of suspended sediment before irradiation(i, k, n) and after irradiation(j, m, o).

Once the disturbance finished, the double-sided flat DGT (Zr-Oxide and AgI gel) was inserted into sediment cores for 24 h to obtain the accumulated concentration of DGT-labile P and S in the pore water of sediment profiles (Ding et al., 2010). Meanwhile, the soil pH meter(PH368) was used to determine the pH, temperature and relative humidity in the sediment. The sediments at a depth of 10 cm below the SWI were cut into five sections at a resolution of 2 cm and freeze-dried for 3 days. The pre-treatment procedures of the amorphous Fe, Al and Mn were referred to Shen's methods (Shen et al., 2023): 1g of freeze-dried sample was added with oxalic acid-ammonium oxalate solution at a soil-water ratio of 1:50(g/mL), and the supernatant was filtered after shaking for 8 h in dark. Then, the supernatant's amorphous Fe, Mn and Al concentrations were determined by AAS and ICP-OES. The subsequent extracted P fractionation steps were according to Hupfer's method (Hupfer et al., 2009). The coefficient of variations(C.V) was used to compare the variations in particle size of different sediments in the vertical direction (Text S2).

3.2.2. Photodegradation experiment

After the pre-incubation period, three groups of columnar sediments were divided into three groups: dark control group, weak light group and strong light group. The visible light exposure was applied after a 2-hour minor disturbance, which was a xenon lamp and the light intensity was adjusted to 40,000 and 85,000 Lux with the 2-hour illumination (Guo et al., 2020; Guo et al., 2023). The overlying water was sampled according to the time gradient before and after illumination (0–2 h) to determine SRP, TDP and TP in the overlying water. 2 g of air-dried sieve samples before and after illumination were extracted with 40 mL of 0.25 M NaOH and 0.05 M EDTA mixed solution for 16 h, and the supernatant was centrifuged at 4 °C for 15 min (Yin et al., 2020). Subsequently, 2 mL was taken to determine TDP and SRP in the supernatant by molybdate spectrophotometry. The remaining filtrated solutions were frozen at −80 °C and then stored in a refrigerator at −20 °C.

Determination of alkaline phosphatase activity: 0.5 g of air-dried sieved sample was placed in a centrifuge tube, added with 0.1 mL of toluene and 2 mL of phosphate buffer, and then added with 0.5 mL of disodium p-nitrophenyl phosphate. After shaking well, it was covered and cultured in an incubator at 36–37 °C for 1 h After the culture was completed, the centrifuge tube was taken out and 0.5 mL $CaCl_2$ and 2 mL NaOH solution were added. After shaking, it was quickly filtered and determined at 420 nm wavelength using a microplate reader.

Electron paramagnetic resonance(EPR) was deployed to determine the reactive oxygen species in the photodegradation process. 0.1 M 5,5-dimethyl-1-pyrroline N-oxide (DMPO) was used to capture •OH in 0, 10 and 30 min after the illumination (Song et al., 2019) whose spectra were recorded by a Bruker spectrometer (Bruker EMXplus-6/1, Germany), with the resonance frequency and the sweep width of 9.8 GHz and 200 G, respectively (Zeng et al., 2022a).

3.3. Batch adsorption experiments

The effect of pH on the adsorption amount of sediment(S), LSS and LSL: 0.5 g of freeze-dried above samples were placed in a series of 25 mL P solutions (1.0 mg/L) with different pH (adjusted to 4–12 with 0.1 M HCl and NaOH). The effect of pH on the P desorption amount of LSS and LSL: freeze-dried samples after P adsorption were placed in 25 mL of pure water with different pH(4–12). After shaking for 2h(180 rpm), the supernatant was filtered by a 0.45-μm microporous filter membrane and the P content was determined. Adsorption efficiencies and amounts were calculated according to the equations in Text S3.

0.5 g LMB was added into a series of 25 mL mixed solution containing P(1 mg/L) at different concentrations(HA: 0, 1, 2, 3, 9, 18 and 36 mg/L and HCO_3^-(in the form of $NaHCO_3$: 0, 50, 100, 200, 800 and 1000 mg/L)(pH=8–10). After shaking for 2h(180 rpm), the supernatant was filtered by the 0.45-μm microporous membrane filter and the P content was determined.

Based on Wen's methods, the algae samples in Xingyun Lake were rinsed with deionized water and placed in a −80 °C refrigerator for freezing and thawing at room temperature three times. After the algae cells were lysed, they were freeze-dried and then dissolved in the deionized water at the water-mass ratio of 100:1(25 °C). After centrifugation, the stocked solution of AOM can be obtained and then a mixed solution with different concentrations (AOM: 0, 1, 2, 3, 9, 18 and 36 mg/L) containing 1 mg/L P (pH=7) can be prepared. Two replicates for each concentration were agitated in a constant temperature oscillator (180 rpm) at 25 °C, followed by filtration using 0.45-μm microporous membrane filters. The concentration of HA and AOM in the Xingyun Lake was determined by UV–visible spectrophotometry at 254 nm (Zhang et al., 2023).

3.4. Characterization

After the microcosm experiment, sediment(S), LSS and LSL samples in a depth of 0–2 cm below the SWI were freeze-dried. The surface morphology and elemental distribution of the LSL and LSS were observed using the thermal field emission SEM (Zeiss, Sigma 300, Germany) and EDS (Oxford Xplore 30). The crystal phase and chemical composition of samples were determined by deploying the XRD (Rigaku SmartLab SE, Japan). The surface composition survey and chemical states of the elements of samples were examined by XPS (ESCALAB250Xi, Thermo Fisher Scientific, USA). Zeta potentials of sediment, LSS and LSL at different pH values(4–12) were tested by Malvern Zeta sizer Nano ZS90. Sediment particle sizes were determined by a particle size analyzer (Mastersizer 2000; Malvern, England) to investigate vertical distribution characteristics of D_{50}, S/V, and proportion of <8, 8–63 and >63 μm particles.

4. Conclusion

Immobilization time and environmental factors in the high-altitude lake could affect the P releasing of sediment, including high alkalinity, organic matter, disturbance and irradiation. Our study demonstrated long-term LMB immobilization caused C accumulation and La depletion in the sediment. $H_nPO_4^{n-3}$ gradually lost its advantages in the process of competing with CO_3^{2-}/HCO_3^- and carboxyl groups for the adsorption sites of La during the immobilization time. High pH and alkalinity ion in the plateau lake has been identified to enhance the P desorption amount and decrease P adsorption amount of the sediment through the zeta potential reduction and electrostatic repulsion enhancement. High concentration of algal-derived organic matter (AOM) could also block the adsorption performance of LMB to P due to looser complexation than humic acid. Further microcosm experiment demonstrated there was a releasing trend of active P contents with the long-term LMB immobilization after major disturbance, while those of the sediment with short-term LMB immobilization after minor disturbance showed a passivation trend related to resuspend particle size's redistribution. Furthermore, ^{31}P NMR and EPR results indicated monoester and diester phosphate photodegraded into orthophosphate and pyrophosphate in the sediment with long-term LMB immobilization via the oxidation of ·OH after the disturbance. Our work emphasized the urgent need for long-term monitoring after the LMB field application and LMB (particle size and dosage) reassessment considering the resuspension caused by disturbance and organic P photodegradation. However, our study was still lack of continuous *in-situ* aging observation and microbial community analysis in the sediment core.

CRediT authorship contribution statement

Jinhui Wang: Writing – original draft, Resources, Investigation. **Lina Chi:** Writing – review & editing, Validation. **Shuai Liu:** Software, Investigation. **Jiao Yin:** Resources, Project administration. **Youlin Zhang:** Visualization, Resources, Project administration, Formal

analysis. **Jian Shen:** Supervision, Conceptualization. **Xinze Wang:** Supervision, Funding acquisition.

Declaration of competing interest

The authors declare that they have no known competing financial interests or personal relationships that could have appeared to influence the work reported in this paper.

Acknowledgments

This research was supported by National Key Research and Development Program of China (2021YFD1700400), Yunnan Provincial Key Research and Development Program (202303AC100017) and Yunnan Fundamental Research Projects (202301AT070001, 202201AU070001). We also appreciate Authority of Ministry of Lake in Yuxi and Shanghai Jiao Tong University Yuxi Lake Joint Research Center.

Supplementary Materials

Supplementary material associated with this article can be found in the online version at doi:10.1016/j.wroa.2024.100272.

Data availability

The data that has been used is confidential

References

Abdellaoui, Y., El Ibrahimi, B., Abou Oualid, H., Kassab, Z., Quintal-Franco, C., Giacoman-Vallejos, G., Gamero-Melo, P., 2021. Iron-zirconium microwave-assisted modification of small-pore zeolite W and its alginate composites for enhanced aqueous removal of As(V) ions: experimental and theoretical studies. Chem. Eng. J. 421, 129909.

Copetti, D., Finsterle, K., Marziali, L., Stefani, F., Tartari, G., Douglas, G., Reitzel, K., Spears, B.M., Winfield, I.J., Crosa, G., D'Haese, P., Yasseri, S., Lürling, M., 2016. Eutrophication management in surface waters using lanthanum modified bentonite: a review. Water Res. 97.

Dadi, T., Schultze, M., Kong, X., Seewald, M., Rinke, K., Friese, K., 2023. Sudden eutrophication of an aluminum sulphate treated lake due to abrupt increase of internal phosphorus loading after three decades of mesotrophy. Water Res. 235, 119824.

Ding, S.M., Xu, D., Sun, Q., Yin, H.B., Zhang, C.S., 2010. Measurement of dissolved reactive phosphorus using the diffusive gradients in thin films technique with a high-capacity binding phase. Environ. Sci. Technol. 44 (21), 8169–8174.

Ding, Y., Qian, Y., Jia, Q., Zhang, J., Zhou, Z., Liu, X., 2023. Quantifying phosphorus levels in water columns equilibrated with sediment particles in shallow lakes: from algae/cyanobacteria-available phosphorus pools to pH response. Sci. Total Environ. 868 (0048–9697), 161694.

Dithmer, L., Nielsen, U.G., Lurling, M., Spears, B.M., Yasseri, S., Lundberg, D., Moore, A., Jensen, N.D., Reitzel, K., 2016. Responses in sediment phosphorus and lanthanum concentrations and composition across 10 lakes following applications of lanthanum modified bentonite. Water Res. 97, 101–110.

Du, H.Y., Cao, Y.X., Li, Z., Li, L.N., Xu, H.C., 2021. Formation and mechanisms of hydroxyl radicals during the oxygenation of sediments in Lake Poyang, China. Water Res. 202.

Egemose, S., Reitzel, K., Andersen, F.Ø., Jensen, H.S., 2013. Resuspension-mediated aluminium and phosphorus distribution in lake sediments after aluminium treatment. Hydrobiologia 701 (1), 79–88.

Funes, A., Alvarez-Manzaneda, I., del Arco, A., de Vicente, J., de Vicente, I., 2021. Evaluating the effect of CFH-12 (R) and Phoslock (R) on phosphorus dynamics during anoxia and resuspension in shallow eutrophic lakes. Environ. Pollut. 269.

Graeber, D., McCarthy, M.J., Shatwell, T., Borchardt, D., Jeppesen, E., Søndergaard, M., Lauridsen, T.L., Davidson, T.A., 2024. Consistent stoichiometric long-term relationships between nutrients and chlorophyll-a across shallow lakes. Nat. Commun. 15 (1), 809.

Guo, M., Li, X., Wang, Y., Zhang, Y., Fu, Q., Huguet, A., Liu, G., 2023. New insights into the mechanism of phosphate release during particulate organic matter photodegradation based on optical and molecular signatures. Water Res., 119954

Guo, M.L., Li, X.L., Song, C.L., Liu, G.L., Zhou, Y.Y., 2020. Photo-induced phosphate release during sediment resuspension in shallow lakes: a potential positive feedback mechanism of eutrophication. Environ. Pollut. 258.

Guo, T., Lin, J., Zhan, Y., 2024. Suppression of phosphorus release from sediment by Vallisneria natans combined with iron- and zirconium-modified bentonites: effectiveness, mechanism, and response of sedimentary microbial communities. J. Environ. Chem. Eng. 12 (5), 113690.

He, Q., Zhao, H., Teng, Z., Wang, Y., Li, M., Hoffmann, M.R., 2022. Phosphate removal and recovery by lanthanum-based adsorbents: a review for current advances. Chemosphere 303, 134987.

Hupfer, M., Gächter, R., Giovanoli, R., 1995. Transformation of phosphorus species in settling seston and during early sediment diagenesis. Aquat. Sci. 57 (4), 1015–1621.

Hupfer, M., Zak, D., Rossberg, R., Herzog, C., Pothig, R., 2009. Evaluation of a well-established sequential phosphorus fractionation technique for use in calcite-rich lake sediments: identification and prevention of artifacts due to apatite formation. Limnol. Oceanogr.-Methods 7, 399–410.

Jalil, A., Li, Y., Du, W., Wang, J., Gao, X., Wang, W., Acharya, K., 2017. Wind-induced flow velocity effects on nutrient concentrations at Eastern Bay of Lake Taihu, China. Environ. Sci. Pollut. Res. 24 (21), 17900–17911.

Jin, J., Xiao, Q., Chen, L., Qiu, Y., Chen, G., 2021. Sex dimorphism of Yunnanilus analis and its habitat adaptation in Xingyun Lake, Yunnan, China(in Chinese). Chin. J. Appl. Ecol. 32 (02), 672–682.

Kong, M., Liu, F., Tao, Y., Wang, P., Wang, C., Zhang, Y., 2020. First attempt for in situ capping with lanthanum modified bentonite (LMB) on the immobilization and transformation of organic phosphorus at the sediment-water interface. Sci. Total Environ. 741, 140342.

Li, C., Ding, S., Ma, X., Wang, Y., Sun, Q., Zhong, Z., Chen, M., Fan, X., 2023. Sediment arsenic remediation by submerged macrophytes via root-released O2 and microbe-mediated arsenic biotransformation. J. Hazard. Mater. 449, 131006.

Li, X.L., Guo, M.L., Duan, X.D., Zhao, J.W., Hua, Y.M., Zhou, Y.Y., Liu, G.L., Dionysiou, D. D., 2019. Distribution of organic phosphorus species in sediment profiles of shallow lakes and its effect on photo-release of phosphate during sediment resuspension. Environ. Int. 130.

Lin, J., Li, Y., Zhan, Y., Wu, X., 2023. Combined amendment and capping of sediment with ferrihydrite and magnetite to control internal phosphorus release. Water Res. 235, 119899.

Liu, M., Ling, H., Wu, D., Su, X., Cao, Z., 2021. Sentinel-2 and Landsat-8 observations for harmful algae blooms in a small Eutrophic Lake. Remote Sens. 13 (21), 4479.

Mallet, M., Barthélémy, K., Ruby, C., Renard, A., Naille, S., 2013. Investigation of phosphate adsorption onto ferrihydrite by X-ray photoelectron spectroscopy. J. Colloid. Interface Sci. 407, 95–101.

Moyle, M., Boyle, J., Bennion, H., Chiverrell, R., 2024. TP or Not TP? successful comparison of two independent methods validates total phosphorus inference for long-term eutrophication studies. Environ. Sci. Technol. 58 (17), 7425–7432.

Münch, M.A., van Kaam, R., As, K., Peiffer, S., Heerdt, G.t., Slomp, C.P., Behrends, T., 2024. Impact of iron addition on phosphorus dynamics in sediments of a shallow peat lake 10 years after treatment. Water Res. 248, 120844.

Pan, F., Liu, H., Guo, Z., Cai, Y., Fu, Y., Wu, J., Wang, B., Gao, A., 2019. Metal/metalloid and phosphorus characteristics in porewater associated with manganese geochemistry: a case study in the Jiulong River Estuary, China. Environ. Pollut. 255, 113134.

Peng, J., Jiang, H., Liu, Q., Green, S.M., Quine, T.A., Liu, H., Qiu, S., Liu, Y., Meersmans, J., 2021. Human activity vs. climate change: distinguishing dominant drivers on LAI dynamics in karst region of southwest China. Sci. Total Environ. 769, 144297.

Reitzel, K., Balslev, K.A., Jensen, H.S., 2017. The influence of lake water alkalinity and humic substances on particle dispersion and lanthanum desorption from a lanthanum modified bentonite. Water Res. 125, 191–200.

Sharpless, C.M., Blough, N.V., 2014. The importance of charge-transfer interactions in determining chromophoric dissolved organic matter (CDOM) optical and photochemical properties. Environ. Sci.-Process. Impacts 16 (4), 654–671.

Shen, X., Li, W., Fan, B., Huang, C., Bai, L., Jiang, H., Xu, H., Wang, C., 2023. Sediment resuspension causes horizontal variations in the distributions of phosphorus (P) and P-inactivating materials with differing P immobilization in different sediment planes. Water Res. 243, 120327.

Sheng, Y., Hu, J., Kukkadapu, R., Guo, D., Zeng, Q., Dong, H., 2023. Inhibition of extracellular enzyme activity by reactive oxygen species upon oxygenation of reduced iron-bearing minerals. Environ. Sci. Technol. 57 (8), 3425–3433.

Song, Y., Fang, G., Zhu, C., Zhu, F., Wu, S., Chen, N., Wu, T., Wang, Y., Gao, J., Zhou, D., 2019. Zero-valent iron activated persulfate remediation of polycyclic aromatic hydrocarbon-contaminated soils: an in situ pilot-scale study. Chem. Eng. J. 355, 65–75.

Wang, J., Sun, Q., Gao, Q., Zheng, H., He, J., Jiang, Y., Liu, Z., Zhang, W., 2022a. Effective immobilization of arsenic in waters and sediments using novel zirconium-loaded lanthanum-modified bentonite capping. J. Environ. Chem. Eng. 10 (2), 107343.

Wang, S., Huang, Y., Wu, Q., Yao, W., Lu, Y., Huang, B., Jin, R., 2024. A review of the application of iron oxides for phosphorus removal and recovery from wastewater. Crit. Rev. Environ. Sci. Technol. 54 (5), 405–423.

Wang, J., Sun, Q., Gao, Q., Sun, X., 2023. Enhanced remediation of new zirconium-loaded attapulgite to As(III) and As(V) and its mechanisms in the aquatic environment. Environ. Sci.: Water Res. Technol. 9 (8), 2099–2111.

Wang, C., Wei, Z., Shen, X., Bai, L., Jiang, H., 2022b. Particle size-related vertical redistribution of phosphorus (P)-inactivating materials induced by resuspension shaped P immobilization in lake sediment profile. Water Res. 213, 118150.

Wang, J., Wu, B., Zheng, X., Ma, J., Yu, W., Chen, B., Chu, C., 2024. Insights into the crystallinity-dependent photochemical productions of reactive oxygen species from iron minerals. Environ. Sci. Technol.

Wang, Y., Ding, S.M., Wang, D., Sun, Q., Lin, J., Shi, L., Chen, M.S., Zhang, C.S., 2017. Static layer: a key to immobilization of phosphorus in sediments amended with lanthanum modified bentonite (Phoslock®). Chem. Eng. J. 325, 49–58.

Wen, S., Lu, Y., Dai, J., Huang, X., An, S., Liu, J., Liu, Z., Du, Y., Zhang, Y., 2023. Stability of organic matter-iron-phosphate associations during abiotic reduction of iron. J. Hazard. Mater. 449, 131016.
Wu, D., Hua, Z., 2014. The effect of vegetation on sediment resuspension and phosphorus release under hydrodynamic disturbance in shallow lakes. Ecol. Eng. 69 (0925–8574), 55–62.
Xu, H.C., Li, Y.N., Liu, J., Du, H.Y., Du, Y.X., Su, Y.L., Jiang, H.L., 2020. Photogeneration and steady-state concentration of hydroxyl radical in river and lake waters along middle-lower Yangtze region, China. Water Res. 176.
Yang, C., Wang, G., Yin, H., 2023. Response of internal phosphorus loading from dredged and inactivated sediment under repeated resuspension in a eutrophic shallow lake. Sci. Total Environ. 868, 161653.
Yin, H., Kong, M., Gu, X., Chen, H., 2017. Removal of arsenic from water by porous charred granulated attapulgite-supported hydrated iron oxide in bath and column modes. J. Clean. Prod. 166, 88–97.
Yin, H., Yang, P., Kong, M., Li, W., 2020. Preparation of the lanthanum–aluminum-amended attapulgite composite as a novel inactivation material to immobilize phosphorus in lake sediment. Environ. Sci. Technol. 54 (18), 11602–11610.
Zawiska, I., Jasiewicz, J., Rzodkiewicz, M., Woszczyk, M., 2023. Relative impact of environmental variables on the lake trophic state highlights the complexity of eutrophication controls. J. Environ. Manage. 345, 118679.
Zeng, Y.B., Chang, F.Q., Wen, X.Y., Duan, L.Z., Zhang, Y., Liu, Q., Zhang, H.C., 2022b. Seasonal variation in the water quality and eutrophication of Lake Xingyun in Southwestern China. Water 14 (22).
Zeng, Y., Li, T., Ding, Y., Fang, G., Wang, X., Ye, B., Ge, L., Gao, J., Wang, Y., Zhou, D., 2022a. Biochar-supported nano-scale zerovalent iron activated persulfate for remediation of aromatic hydrocarbon-contaminated soil: an in-situ pilot-scale study. Biochar 4 (1).
Zhan, Y.H., Qiu, B., Lin, J.W., 2023. Effect of common ions aging treatment on adsorption of phosphate onto and control of phosphorus release from sediment by lanthanum-modified bentonite. J. Environ. Manage. 341.
Zhang, Y., Shen, J., Feng, J., Li, X., Liu, H., Wang, X., 2023. Composition, distribution, and source of organic carbon in surface sediments of Erhai Lake, China. Sci. Total Environ. 858.
Zhou, X.F., 2016. Characterization and sources of sedimentary organic matter in Xingyun Lake, Jiangchuan, Yunnan, China. Environ. Earth Sci. 75 (13).